Geomechanics for Energy and the Environment 40 (2024) 100613

Contents lists available at ScienceDirect

Geomechanics for Energy and the Environment

journal homepage: www.elsevier.com/locate/gete

Comparison between new enhanced thermal response test methods for underground heat exchanger sizing

A. Galgaro [a], R. Da Re [b], A. Carrera [a], E. Di Sipio [c], G. Dalla Santa [b,d,*]

[a] Department of Geosciences, Università degli Studi di Padova, Italy
[b] Dept. of Civil, Environmental and Architectural Engineering ICEA, Università degli Studi di Padova, Italy
[c] Dept. Information Engineering DEI, Università degli Studi di Padova, Italy
[d] Dept. of Industrial Engineering DII, Università degli Studi di Padova, Italy

ARTICLE INFO

Keywords:
BHE
Enhanced Thermal Response Test
Hybrid fiber optic
GEOsniff
Thermal conductivity
Distributed Thermal Response Test DTRT

ABSTRACT

For the efficient design and implementation of a Ground Source Heat Pump (GSHP) system, the local subsoil stands as the core element. Alongside the conventional Thermal Response Test (TRT), recent research has developed improved approaches that garner more detailed information about ground thermal properties. One such technique is the fiber optic-based distributed thermal sensing. It relies on copper wires to thermally stimulate the ground, while optical fibers collect temperature variations over time along the cable. Another pioneering technology, the enhanced GEOsniff (produced by enOware GmbH), enables high-resolution, spatially-distributed representation of subsoil thermal properties along the Borehole Heat Exchanger (BHE) via wireless data transmission. This study compares and discusses data acquired through these two innovative techniques at the new campus for the humanities of the University of Padova, situated in Northern Italy's Eastern Po river plain. The findings are further juxtaposed with conventional TRT results, in terms of thermal conductivity and borehole thermal resistance. The thermal conductivity vertical profiles are also compared with direct measurements conducted on samples. These advanced techniques show promise in aiding the optimization of borehole length design, particularly in geological settings of heightened complexity.

1. Introduction

As the thermal efficiency of Borehole Heat Exchangers (BHEs) varies based on site-specific factors, planning a Ground Source Heat Pump (GSHP) system typically necessitates understanding the ground's thermal properties. These properties are shaped by the local stratigraphic sequence and hydrogeological conditions. Assessing the local heat exchange capability becomes crucial for appropriately sizing a GSHP system, both in terms of energy efficiency and financial viability. Estimating variations in ground thermal conductivity (TC) across depth, alongside its undisturbed temperature, becomes imperative in properly designing the BHEs' field and optimizing the performance of ground heat exchangers.

The Thermal Response Test (TRT) is a well-established experimental procedure, initially developed by [14]Eklöf and Gehlin[14] and[6], which enables the determination of the equivalent thermal conductivity of the local subsoil by directly testing a borehole. However, the conventional TRT method provides a single value for the ground's undisturbed temperature and a mean TC value over the entire testing BHE length, lacking the ability to detect variations in thermo-physical parameters with depth or distinguish contributions from different geological layers crossed by the geothermal heat exchanging borehole.

Within a stratigraphic sequence, distinct layers may exhibit differing thermal properties due to factors such as groundwater presence and flow rate, sediment granulometry, mineral contents, density, texture and porosity[24]. Evaluating the different ground contributions to the BHE thermal capability, can provide high-quality, useful information for optimum BHE design. This assessment aids in determining the most suitable borehole length (maximum reached depth) and number, achieving peak heat exchange capability while minimizing initial implementation costs for the entire geothermal plant maximizing its energy efficiency and optimizing the economic investment[7,37].

In the 1990s, depth-resolved Thermal Response Tests (TRTs) emerged[15,1,2] to capture temperature variations over time at multiple depths along the entire borehole. Temperature measurements are obtained either i) through sensors distributed at specific depths, such as

* Corresponding author at: Dept. of Civil, Environmental and Architectural Engineering ICEA, Università degli Studi di Padova, Italy.
E-mail address: giorgia.dallasanta@unipd.it (G. Dalla Santa).

https://doi.org/10.1016/j.gete.2024.100613
Received 27 March 2024; Received in revised form 3 October 2024; Accepted 22 October 2024
Available online 28 October 2024

thermocouples, or ii) by using moving wireless probes, or iii) via fiber optic cables inserted into the heat exchanger tube within the water or sealed in the sealing grout. Paired with induced thermal stimulation, this depth-distributed measurement of temperature changes over time enables the evaluation of thermal conductivity across various geological layers along the borehole depth. Wilke et al.[38] extensively reviewed the significant technological and historical advancements in innovative TRT methods concerning test setups, assessment methods, and geological applications utilizing optical fiber cables, hybrid cables, and wireless probes.

Recently, depth-resolved TRTs have been categorized into two classes: Distributed Thermal Response Test (DTRT) and Enhanced Thermal Response Test (ETRT) [4,3]. In a DTRT, temperature is measured with sensors at discrete intervals (providing numerous measuring points at different depths), while heating is typically supplied by an external source, often heated circulating water from an external tank using an electrical resistance as heat stimulator, akin to conventional TRTs. Conversely, an Enhanced Thermal Response Test (ETRT) involves directly inserting a copper cable into the borehole and heating it by injecting a constant electric power, ensuring uniform heating throughout the borehole depth, due to Joule thermal effect. Generally, an ETRT is conducted with hybrid fiber optic cables (FO-ETRT), which combine heating copper wires with temperature measuring optic fibers, allowing temperature measurements along the whole depth, thus effectively being an EDTRT [40,39].

A first comparison between the results obtained from a traditional TRT and an ETRT conducted in a Double-U borehole in Vienna is discussed by De Sousa Figueira et al. [13]. In this case, the ETRT was able to detect a notable increase in thermal conductivity values, peaking at 3.9 W/(m·K) locally, between approximately 8- and 11-meters deep. This increase was attributed to the presence of groundwater flow. The difference between the average thermal conductivity values along the entire profile was found to be 8 %.

Recently, Albers et al. [3] introduced new techniques for evaluating ETRT datasets in environments with significant groundwater flow ($> 0.2\ m\ d^{-1}$). They compared various approaches for determining the specific heat load of the ETRT and tested new methods to take into account the effects of groundwater flow for a more accurate assessment of thermal conductivity.

Recent advancements in ETRT techniques have introduced groundbreaking approaches, such as the wireless data transmission technology GEOsniff® (produced by enOware GmbH,https://www.enoware.de/en/), referred to as Wireless Enhanced Thermal Response Test (W-ETRT). This method utilizes sensors—20mm-diameter marbles equipped with pressure and temperature transducers—paired with a data storage and wireless transmission system. Released at regular time intervals within the testing BHE and filled with water, each marble drops slowly at a constant rate into the BHE filled with water, enabling the measurement of water temperature variations over time at different depths, indirectly estimated by a hydro-pressure sensor. This facilitates the identification of layers with distinct thermal conductivity values linked to specific hydrogeological or lithological conditions. Consequently, GEOsniff® technology enables a high-resolution, spatially-distributed representation of subsoil thermal properties along the BHE[32,4].

This paper presents data acquired from two distinct Enhanced and Distributed Thermal Response Tests conducted at the same testing site situated in Padova, within a low-alluvial plain geological setting (in the Po plain, Northern Italy). The first test (I) employs hybrid fiber optic cables (FO-ETRT), sealed for 124 m within a 130 m deep monitoring well, while the second test (II) utilizes wireless sensors (W-ETRT) placed in a double-U borehole located 1 m away and extending 120 m deep.

The outputs obtained from the FO-ETRT and W-ETRT campaigns have been compared and analyzed in terms of undisturbed temperature profiles, thermal conductivity of significant geological layers, and borehole thermal resistance. These results have been further compared with data obtained from conventional TRT. Furthermore, this paper delves into a comparison of the primary components, complexity of the applied devices, measurement duration and data analysis associated with each technique.

These innovative techniques promise to provide the best support for designing and sizing borehole heat exchanger fields, particularly in complex geological contexts.

2. The study case

The measurements were conducted at the University of Padova's new humanistic campus situated in the northeastern region of Italy. This site, located within the historic urban core of Padova, underwent renovations in 2019 (Fig. 1). The renovation project encompassed the refurbishment of its 17 buildings and introduced a modern hybrid heating and cooling system aligned with the renewable energy objectives supported by the EU-funded project Geo4Civhic (visit https://geo4civhic.eu/ for more details).

The implemented system comprises two geothermal heat pumps catering to the base thermal load (approximately 170 kW) along with two air/water heat pumps addressing peak demands. The borehole field consists of 60 BHEs extending 120 m, spaced 7 m apart. They are equipped with double-U tubes, strategically placed across three courtyards. The collective volume of the buildings amounts to 61,500 m^3, accompanied by a combined heating/cooling floor area of 16,654 m^2.

Although the system became operational in July 2019, its full functionality has been hindered by limitations imposed due to the SARS-CoV-2 pandemic.

Three monitoring wells were strategically placed - one upstream, another downstream, and the third positioned in the center of the borefield, indicated by the crosses in Fig. 1b - to monitor underground thermal conditions both before and during plant operation in order to detect potential thermal plumes[29]. Each monitoring well was equipped with specific thermal sensors, referred to as MUMS (Modular Underground Monitoring System), set at known depths within the wells (approximately every 10 m) down to 130 m. These sensors enable temperature measurements of the ground at various depths from the surface over time (a detailed description is provided in Section 3.4).

In addition, the central monitoring well (represented by a red cross in Fig. 1b), critical for assessing heat exchange processes, was fitted with a hybrid cable. This cable comprises an optical fiber capable of high-resolution temperature measurements across time and space, combined with copper heating cables grouted into the well down to a depth of 124 m, that is 4 m deeper than the boreholes. The FO-ETRT was conducted exactly inside the monitoring well, which sits just 2 m away from the closest 120 m-long BHE (black circle in Fig. 1b), where the conventional TRT was performed. Differently, the W-ETRT tests were performed in an adjacent BHE (indicated by an orange circle in Fig. 1b).

Currently, the MUMS system is constantly running to monitor ground temperature affected by the BHEs' operation and the fiber optic in the central monitoring well operates passively and can acquire data on demand to perform further FO-ETRTs.

2.1. Site geological assessment

Understanding the composition of various layers constituting the underground where the boreholes are installed is pivotal to enhancing the performance of these heat exchangers. Stratigraphy, coupled with TRT results, allows for a more precise assessment of thermal conductivity behaviour across different depths. The subsoil geotechnical investigation reached a depth of 130 m, revealing a predominant presence of sand and silt layers (Fig. 2 shows the simplified stratigraphy). The deposits exhibit a complex heterogeneity, characterized by a repeated and alternating pattern of coarse sand/gravel, sand, silt layers alternate with clay and sporadic peat deposits. This lithological sequence is characteristic of the Po Valley region alluvial deposits where the site is located, comprising Quaternary fluvial and alluvial deposits of

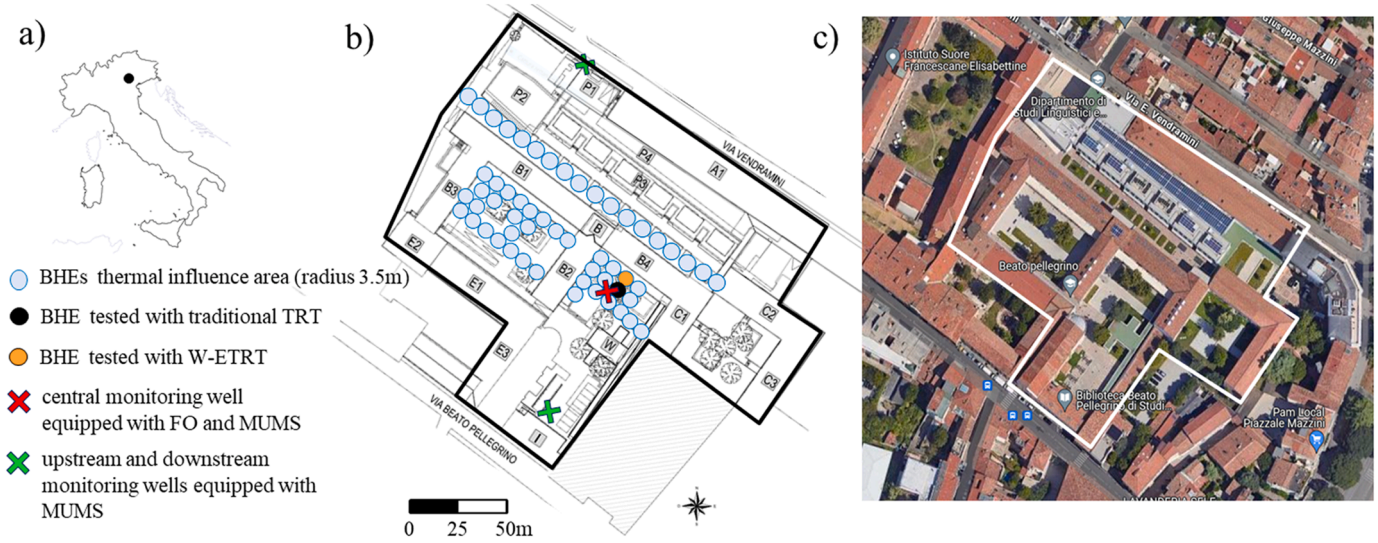

Fig. 1. a) Location of the city of Padova; b) the BHE plant installed in the new Humanities campus of the University of Padova. Each BHE is represented with its thermal influence area measuring 3.5 m in diameter. The distance between BHEs is maintained at 7 m to prevent thermal interference; c) view of the complex of buildings and courtyards of the refurbished campus (from GoogleMaps, dati cartografici2024).

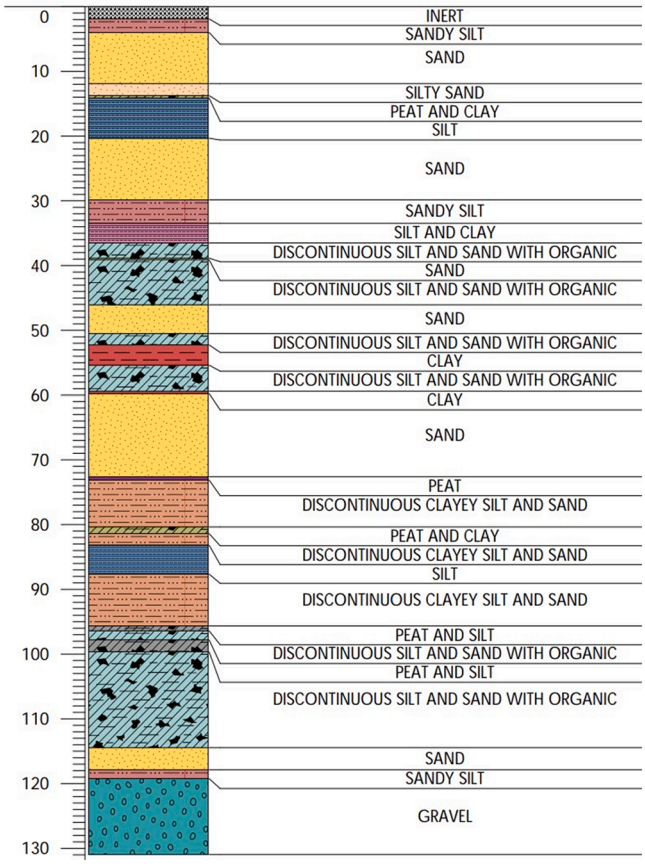

Fig. 2. Simplified stratigraphy of the site, obtained by the well corings.

continental and shallow marine environment origins, the most sensible to low temperatures [10,9]. The deposits were formed during a period spanning from the late Pleistocene to the Holocene. The near-surface phreatic aquifer maintains a water table at a depth of 1.5 m. Stratigraphic analysis indicates a multilayered aquifer structure within the subsoil, consisting of several aquifers partially or fully confined by fine layers. Consequently, the levels intersected by the borehole are considered fully saturated. Notably, the sandy layer at 60–70 m depth shows evidence of groundwater flow. In addition, at the lower part of the sequence lies a substantial gravel deposit, notable for its groundwater flow that significantly impacts the heat exchange capacity, due to advection contribution[16]; however, only a fraction of this deeper layer affected by meaningful groundwater flow directly affects the BHEs, as they are buried at a depth of 120 m. For a more detailed insight into the stratigraphic sequence, a comprehensive description is available in[25].

All extracted samples underwent comprehensive geotechnical classification laboratory tests, including sieve analysis, Atterberg Limits assessment, and mineralogical composition analysis. Additionally, over 80 direct measurements of thermal conductivity were performed on the cores [11,12] using the Isomet 2114 Thermal Properties Analyzer by Applied Precision (measuring range: 0.015–0.70 $Wm^{-1}K^{-1}$ accuracy: 5 % reading + 0.001 Wm^{-1} K^{-1} / 0.70–6.0 Wm^{-1} K^{-1} accuracy: 10 % reading).

3. Matherials and methods

3.1. Conventional Thermal Response Test (TRT)

As already known, in the conventional TRT the undisturbed ground temperature is first assessed. After this, an external source applies a constant heat rate to a circulating fluid within a test Borehole Heat Exchanger (BHE), typically for a 72-hour period. Over time, temperatures of the inlet and outlet heat carrier fluid are recorded, alongside flow rate, ambient temperature, and the electric input power to the heater and pump.

Upon completion of the test, inverse modeling of the mean fluid temperature profile estimates pertinent parameters: the average thermal conductivity (λ_{eq}) across the entire stratigraphy, the thermal resistance (R_b) of the borehole/grout/ground, and the undisturbed soil temperature (T_g).

The equipment comprises two modules (refer to Fig. 3a). The first is called the *measurement module* and includes the following: i) a hydraulic circuit with a circulator and various valves for regulation, interception, and safety; ii) a measurement system incorporating two PT100 temperature probes for the fluid, a PT100 temperature probe for outdoor air, an electromagnetic flow rate flowmeter, and a pressure transmitter; iii) a data acquisition and storage system.

The second module is specific to executing the TRT and includes i) a

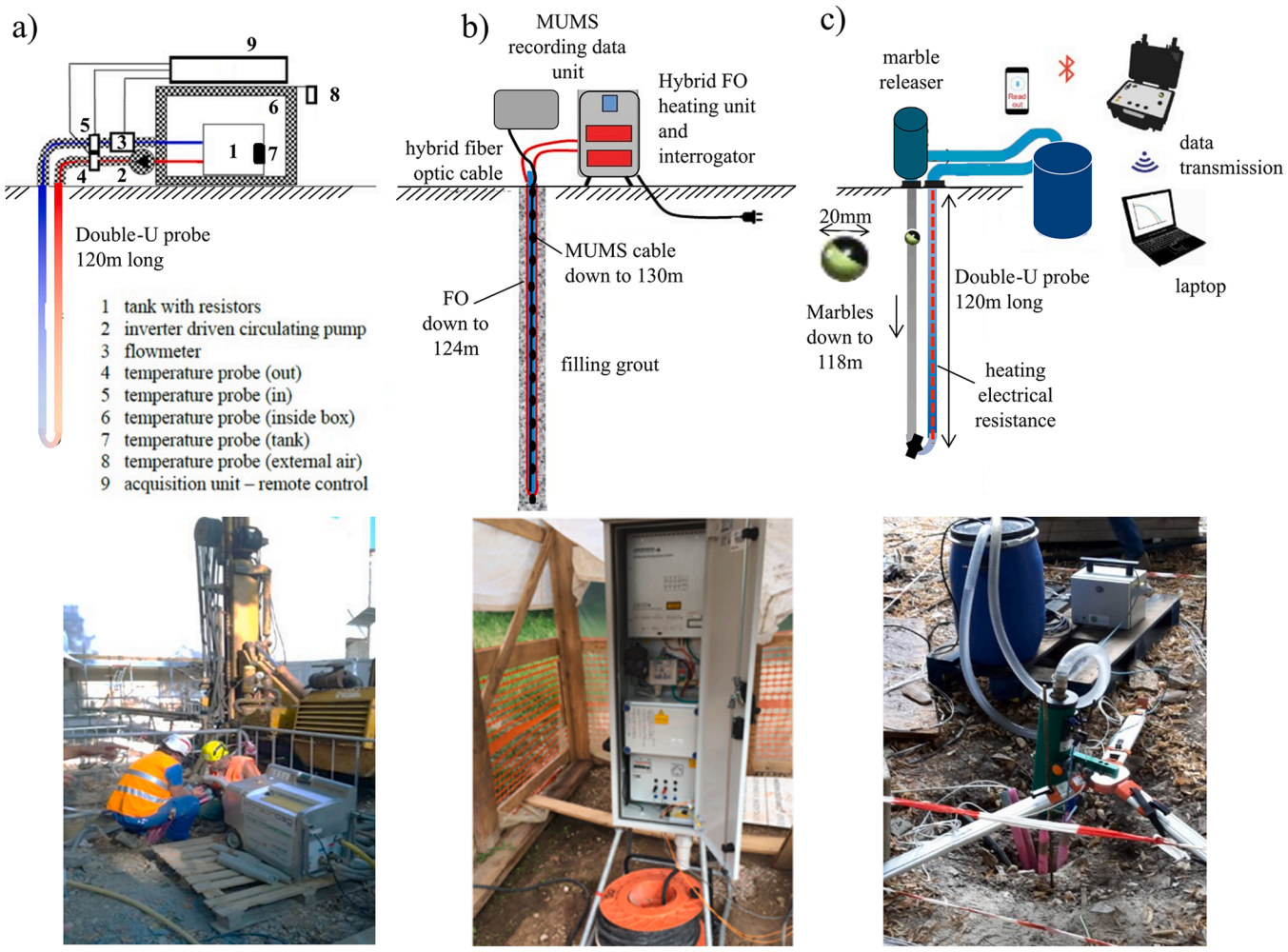

Fig. 3. Comparison among the main components of the applied devices: a) conventional TRT device; b) DTS interrogator used for the ETRT with hybrid fiber optic cable (FO-ETRT); c) warm water tank, marbles storage and detector used for the ETRT wireless sensor system (W-ETRT).

heat exchanger and ii) a hydraulic circuit with a circulator, an expansion vessel, and safety shut-off valves. This system supplies a constant known thermal power via electrical resistances while recording inlet and outlet temperature time series from the borehole heat exchanger.

During the borefield design phase, for determining the optimum BHE field dimensions, comprehensive knowledge of fluid properties, geometric and thermal pipe characteristics, ground stratigraphy, and undisturbed ground temperature is essential.

In this study case, the conventional TRT took place on September 16, 2016, in the borehole represented by a black circle in Fig. 1b. The TRT provided the undisturbed ground temperature, and the value of the equivalent thermal conductivity through 3 days of heating test. Furthermore, the ground heating during the conventional TRT was monitored using a temporary system inserted into the adjacent (2 m apart) 120 m monitoring well, represented by a red cross in Fig. 1b, before sealing inside the fiber optic cable (see Section 3.2). These measurements are labeled as 'well-log 16.09.2016' in Fig. 7.

Table 1 reports the comparison among the main characteristics of the conducted tests.

3.2. ETRT with hybrid fiber optic cable (FO-ETRT)

The Enhanced Thermal Response Test (ETRT) conducted using a fiber optic cable is a method that enables spatially distributed temperature sensing during and after direct thermal stimulation of the ground. This approach allows for the determination of local ground properties along the entire borehole length via high-resolution fiber optic measurements. Unlike the conventional TRT, this technique offers highly localized resolution in determining effective thermal conductivity, facilitating the optimization of borehole design in terms of depth, number, and size [23].

Here, the hybrid fiberglass-copper cable was sealed into the monitoring well after the drilling operations and using a thermally enhanced grout (with a thermal conductivity around 2 $Wm^{-1}K^{-1}$). Alternatively, an ETRT may be performed by inserting the cable into one leg of the BHE filled with water[35]. During the measurement campaign, the fiber signal detector is connected at one or both ends of the fiber cable and requires electrical supply (refer to Fig. 3b). Aside from this, there are no electronics, sensors, electrical wires, or connections along the cable.

The FO-ETRT technique operates by heating the copper wires with constant electric power injection, inducing thermal stimulation of the ground through their intrinsic resistivity (Joule effect). Concurrently, optical fibers measure temperature variations along the cable at high spatial and temporal resolutions.

This technique operates based on Raman Optical Time-Domain Reflectometry, where an optical pulse injected into the fiber-cable triggers molecular vibrations within the silica glass, producing three backscattered wavelength peaks. The first peak, Rayleigh signal, maintains the same wavelength as the input, while the other two, the Raman peaks (Stokes and Anti-Stokes), are temperature-dependent shifts[31]. The energy ratio between the Anti-Stokes and Stokes bands enables the calculation of temperature at its origin, compensating for losses along

the sensing fiber. The evaluation of measured temperature curves *T(z)* can be obtained using Eq. 1:

$$T(z) = T_{ref}\left(1 + \frac{\Delta\alpha * z}{\ln\frac{C^+}{C^-}} + \frac{\ln\frac{I^+}{I^-}}{\ln\frac{C^+}{C^-}}\right) \quad (1)$$

with:

- T(z): temperature along the fiber wire at depth z [K];
- T_{ref}: reference temperature [K];
- Δα: differential attenuation between Stokes and anti-Stokes backscatter [m^{-1}];
- I^+: intensity of Stokes band;
- I^-: intensity of anti-Stokes band;
- C^+,C^-: constants relating to sensitivity of I^+ and I^- to temperature.

According to other authors[31], the sensing fiber can be probed in two configurations. In the single-ended setup, probing occurs from one end only, extending the sensing range but without distinguishing losses experienced in the measurement's Stokes and anti-Stokes signals. Conversely, the double-ended configuration resolves this issue by probing the fiber in both forward and backward directions, allowing differentiation of wavelength-dependent losses and ensuring inherent robustness.

For this study, we utilized a commercially distributed thermal sensing device (APsensing GeoDTS, model N4388A) in a double-ended configuration. Initial measurements acquired the undisturbed soil temperature passively using the DTS. Subsequently, during a 3-day current injection period (5th to 8th March 2018), temperature behavior of the well and surrounding ground was measured, continuing until thermal recovery (13th March 2018). The overall assumption is that the specific heat load remains constant along the length of the heating cable. Therefore, the heat load was determined by monitoring the current during the ETRT and subsequently calculating the average heat load over the entire heating period, as recommended by Albers et al.[3]. The heating power during this phase ranged between 3.7 and 4 kW, with fluctuations due to nearby building power usage and variations from day to night. The temperature field was sampled every 0.5 m along the sensing fiber at a spatial resolution of 1 m, with a time sampling interval of 2 minutes and temperature accuracy within tenths of Celsius degrees. Therefore, the data are provided at intervals of 0.5 m, with each measurement representing an average value across 1 m (0.5 m above and 0.5 m below the declared point). A summary of this data is presented in Table 1.

As already mentioned, the FO-ETRT was conducted in the monitoring well, characterized by the section depicted in Fig. 4a. The total length of the fiber cable is 276 m, with 248 m sealed in a U configuration within the well (124 m in an up-down and 124 m in a down-up arrangement). The dataset comprises hundreds of temperature traces collected over 8–10 days at each 'sensor depth. The raw temperature data collected along the U-shaped cable were analyzed by distinguishing between data measured in the up-down and down-up legs of the cable. The values recorded at the same depth were then averaged. Only the temperatures measured underground were considered, excluding those taken outside the well. Additionally, a smoothing filter with a moving average of 32 points was applied using MATLAB to reduce the signal-to-noise ratio and enhance data interpretation.

The hybrid fiber optic cable sealed in the monitoring well facilitated three ETRT campaigns lasting approximately 10 days each in March 2018, November 2018, and June 2019, as discussed and compared in Dalla Santa et al.[11]. For this discussion, we focus solely on the first

Table 1
Main characteristics of the performed tests.

	conventional TRT	FO-ETRT	W-ETRT
Instrument	GEOgert 2.0	APsensing GeoDTS - model N4388A	enOware GeoSniff® AUTO-TRT KIT
Tested well/BHE	double-U PE-Xa PN 15 borehole "S28/C05"	Central monitoring well	double-U PE-Xa PN 15 borehole "S28/C05"
Well/BHE geometry	External diameter: 152 mmTotal length: 120 mSealing grout: Fassageo100 (λ = 2 $Wm^{-1}K^{-1}$ *)	External diameter: 152 mmTotal length: 130 mSealing grout: Thermocem plus (λ = 2 $Wm^{-1}K^{-1}$ *)	External diameter: 152 mmTotal length: 120 mSealing grout: Fassageo100 (λ = 2 $Wm^{-1}K^{-1}$ *)
Campaign date	16–20 September 2016	5–13 March 2018	11–16 July 2018
Duration	30 min in undisturbed conditions +78h (heating)	30 min in undisturbed conditions+73.7h (heating) + 96 h (recovery)	30 min in undisturbed conditions+72.5h (heating) + 28 h (recovery)
Acquired data	temperature of the water entering and exiting the double-U tubes	Ground temperature was recorded along the entire well, with readings provided every 0.5 m, averaged over a 1 m interval around each measurement point	Vertical profile of the water temperature within the borehole, established in equilibrium with the surrounding ground.The instantaneous marble depth is determined based on the recorded pressure.
Acquisition frequency	60 s	2 min-time sampling	6 temperature vertical profiles at predetermined intervals: 1 undisturbed + 4 during the heating phase (at 17, 23, 33, 73 h) + 1 measure achieved 28 h post-heating cessation
Spatial accuracy	1 unique temperature curve over time for the entire BHE	1 temperature curve every 1 m of the well depth	1 temperature curve derived from interpolating the last 3 measurements during heating, at 0.1 m intervals of the well depth.
Measuring accuracy	The temperature sensor used is RTD PT100 cl.1/3 DIN, with a resolution < 0.01 °C in a temperature range of - 55/+110 °C	+−0.04 °C	Temperature sensor resolution (−10 <T<30 °C): < ±0.05 °CPressure sensor: resolution 1.0 mbar, accuracy ± 300 mbar
Heating method	Flowing of hot water, heated by electrical resistances in a outside water tank	Heating cable sealed grouted into the well, together with the measuring fiber optic	Heating cable inserted into the water within one leg of the U-tube (while the marbles float in the other leg).
Electric power supply	6.9 kW	6.4 kW	2.74 kW
Heat rate generated (due to cable length and diameter)	58 W/m	23 W/m	18 W/m
Max ΔT among undisturbed and end of heating phase:	18.0 °C	22.8 °C	5.63 °C

* see[27]

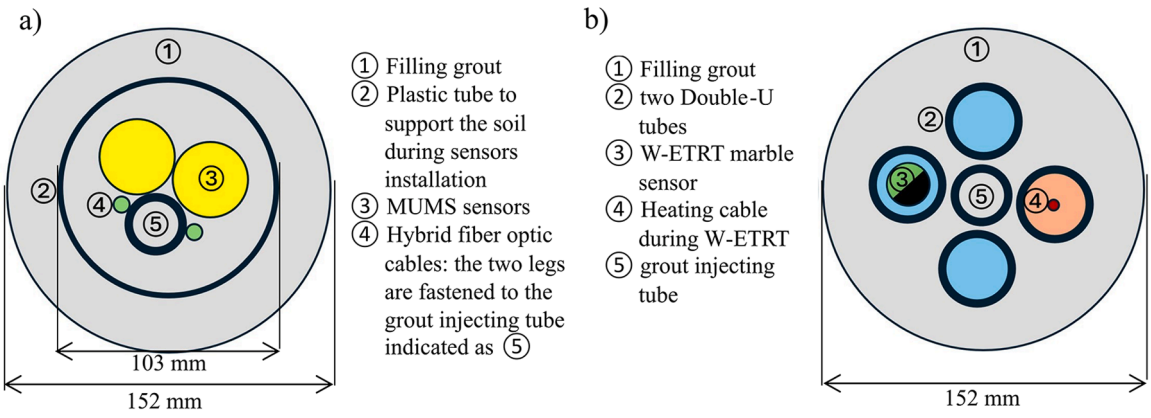

Fig. 4. a) Cross section of the monitoring well, with the hybrid fiber optic cable and MUMS. b) Cross section of the double-U tubes where both the traditional TRT and the W-ETRT have been performed, indicated in Fig. 1b by a black circle.

campaign, aligning it for comparison with results obtained via the W-ETRT due to its closer time proximity.

3.3. ETRT wireless sensor system (W-ETRT)

Over recent years, in emulation of distributed temperature sensing systems, enhanced methodologies for conducting a modified TRT have emerged, exemplified by the pioneering wireless data transmission technology called GEOsniff® (enOware GmbH).

This Enhanced Thermal Response Test involves heat injection into the ground via one or more heating cables inserted into the water within the BHE. Alternatively, thermal stimulation of the subsoil can occur by circulating warm water into the borehole tubes, heated externally similarly to conventional TRT procedures. The W-ETRT measures the vertical ground temperature distribution and its temporal evolution using isolated sensors released at specified intervals inside the BHE, sinking down all along the length of one leg of the U-tube.

This method utilizes sensors in the form of 20mm-diameter marbles equipped with pre-calibrated pressure (±300 mbar (10 bar, 0–40 °C)) and temperature (± 0.05 °C (-10 °C to +30 °C)) transducers, coupled with a data storage and wireless transmission system. Released at regular intervals into the tested BHE and submerged in water, each marble glides freely, enabling measurement of water temperature along its length. By elaborating temperature evolution over time, it is possible to identify geological layers with distinct thermal conductivity values related to specific hydrogeological or geological conditions. Consequently, GEOsniff® technology provides high-resolution spatially-distributed insights into subsoil thermal behavior along the stratigraphic sequence, albeit at predetermined temporal intervals.

The equipment employed is notably simple and lightweight (refer to Fig. 3c). It consists of a heated water tank or a heating cable to be inserted into one leg of the double-U borehole and a 'marble storage' fitted onto a valve connected at one of the two ends of the U-tube extending from the ground, housing the sensors. It can accommodate up to six or eight different marbles, enabling an equivalent number of measurements at various times. Once introduced into the U-tubes, the marble descends at a reduced speed due to its slightly higher density (1700 kg/m^3) than the water filling the U-tube, descending at a rate of 6.5 m/min, remotely controlled via two Wi-Fi antennas by a control unit. In order to avoid any potential obstruction, all the marbles stop almost 2 m before the U-bend of the U-tube, and finally they are collected at the end of the measurement.

The first marble has to be released before the thermal excitation, to reconstruct the subsoil's undisturbed temperature profile, aiding in understanding the natural thermal gradient and identifying potential hydrogeological phenomena. Subsequent profiles are obtained during the thermal excitation phase initiated by the heating cable. The test duration mirrors that of a conventional TRT: after the warm-up phase, a final measurement is usually taken during the recovery phase, 24 hours after termination of the thermal excitation.

In this study, the GEOSNIFF survey was conducted in the double-U borehole (represented by the orange circle in Fig. 1b) beside the one used for the conventional TRT, from July 11th to 16th, 2018. The cross section of the tested borehole is depicted in Fig. 4b, compared to the one of the monitoring well.

In addition, two PT100 temperature probes were affixed outside the marble storage: one for air temperature measurements and another inserted into the borehole, coupled with the heating cable, to check its functionality. As outlined in Table 1, in this case only 6 marbles were utilized: the first measured the undisturbed temperature vertical profile before the heating phase commenced. Subsequent measurements were taken during the heating phase, at 17, 23, 33, and 73 hours after the heating phase initiation. The sixth measurement occurred 28 hours post-heating cessation. The initial measurement during the heating phase commenced after 17 hours, considering a 12-hour period to reach a semi-stationary state. These intervals could vary, but they must include one marble at the start (to obtain the undisturbed temperature), two or three during the central part of the heating phase, and one at the end, after 24 h of the heating phase end. While the optimal choice of intervals may not have been identified yet, the resulting thermal conductivity of each soil layer should remain consistent.

Each marble provided a vertical temperature profile. From the 6 temperature profiles, temperature data were extracted every 10 cm along the borehole, resulting in 6 temperature measurements acquired at fixed times for each depth.

By interpolating the curve derived from the last two or three temperatures recorded during the heating phase (recorded by the marbles released at 23, 33 and 73 hours after heating initiation) at each depth, we obtained the thermal conductivity of the ground surrounding the well at different depths, allowing for the assessment of λ across each geological layer. The investigation ceased at a depth of 118 m to prevent the GeoSniff® measurement pigs from encountering obstruction at the bottom of the U-tube (120 m).

In Table 1 all the main characteristics of this method are reported. Please note the difference in spatial resolution, temporal sampling, measurement accuracy and heating power among the two innovative techniques and the traditional TRT.

3.4. Modular Underground Monitoring System (MUMS)

The acronym MUMS stands for Modular Underground Monitoring System, an innovative technology recently developed by ASE srl for continuous and remote monitoring of underground temperatures. The sensors constituting the thermal array, known as Thermo Links, total 14

in number (Fig. 5). They are encapsulated in an epoxy resin capsule and are linked by an electric cable and a mechanical resistance wire made of aramid fiber. These digital thermocouples possess an electronic board interconnected via an RS485 line, enabling streamlined connectivity through a single cable. This arrangement forms a chain with sensors placed proportionally to cover the required depth. The cable connects to a GEI G801 control unit, systematically querying all nodes at 15-minute intervals and storing the acquired data in an SD card. The memory card can be manually removed to facilitate data downloads and subsequent processing.

In our study case, two chains of 14 sensors, each spanning a depth of approximately 130 m, were installed for each monitoring well (Upstream, Downstream and Central wells, see Fig. 1b). In both the Upstream and Downstream wells, the two MUMS chains were inserted to ensure that the sensors of each chain are at the same depth, spaced approximately 10 m apart, except for the shallower sensors positioned at depths of 1, 2, 3, 5, 8, and 10 m. This redundancy was implemented to ensure measurement coverage in case of malfunctions. However, in the Central well (the same of the fiber optic cable), the two chains were inserted alternately, spacing the sensors approximately 5 m apart and sealed with ThermoCem Plus grout. The monitoring activities started at 03/11/2017 for the Central well and are currently ongoing to track the seasonal and multi-year progression of the thermal plume generated in the ground by the operational borefield.

Even though the MUMS chains have been installed for monitoring purposes, the data acquired by the MUMS chains placed within the Central well are here analyzed to assess both the undisturbed ground temperature and the thermal conductivity at the corresponding depths by utilizing the data recorded during the thermal stimulation generated by the FO-ETRT performed in the same borehole (the central monitoring well), to have an additional extra/external dataset to compare with the methods analyzed in this work

3.5. Data analysis - Line Source Theory

Due to its simplicity and effectiveness, the most commonly utilized analytical model for interpretation of TRT data is the Infinite Line Source (ILS). The development of this method can be attributed to the Kelvin line heat source theory developed in the late 19th century [21] followed by the Carlsaw solutions in 1921 until the 1950s when Ingersoll applied that principle to borehole heat exchangers[18,19]. This method is widely used by the majority of researchers in the field and is recommended in major technical guidelines [28,34,7,33]

This model represents the BHE as an infinite linear heat source embedded in an infinite homogeneous medium characterized by a uniform initial temperature and assumes that the heat source releases a constant heat power during the test. The heat transfer process is considered to take place solely through conduction, and the thermal behavior is assumed symmetric only in the radial direction from the borehole axis.

The analytical solution of the infinite line source model for conduction for a real borehole is expressed in the following equations:

$$T(r,t) - \quad T_{ug} = \quad \frac{Q}{4\pi\lambda_s H} E(u) + qR_b \tag{2}$$

$$E(u) = \int_u^{\infty} \frac{e^{-u}}{u} du \tag{3}$$

where

$$u = \quad \frac{r_b^2}{4\alpha_s t} = \quad \frac{1}{4F_0} \tag{4}$$

$$T(t) - T_{ug} = \frac{q}{4\pi\lambda} \ln(t) + q\left[R_b^* + \frac{1}{4\pi\lambda} \ln\left(\frac{4\alpha}{r_b^2}\right) - \gamma\right] \tag{5}$$

with:

- $T(t)$: average measured temperature in function of time t [°C];
- T_{ug}: undisturbed ground temperature [°C];
- t: time [s];
- Q: Heat power provided by the heater [W]
- H: Borehole length [m]
- q: linear thermal power injected in the borehole = Q/H [W/m];
- r_b: radius of the perforation, supposed constant and equal to the outer diameter of the drill [m];
- α: thermal diffusivity of the soil [m^2/s];
- γ: Euler constant, equal to 0.57721;
- λ: thermal conductivity of the soil [W/(m·K)];
- R_b^*: borehole thermal resistance [(m·K) /W].
- $E(u)$: exponential integral function or Theis well function

Where F_0 is the Fourier number, a dimensionless parameter that characterizes the heat conduction; as F_0 assumes the value of 1, this means that the released heat reaches the external radius of the borehole (r_b). For practical applications, Banks[7] suggested values of $F_0 \geq 5$ to apply the ILS as an analytical method for the TRT results, thus indicating a minimum duration of the heating period to overcome the borehole resistance and involve a significant volume of surrounding ground in the heating phase. Consequently, for a height to radius ratio greater than 1000 and sufficiently long time (t), it is possible to approximate the solution of Eq. 3 at the first order[39], using Eq. 4, thus obtaining the analytical solution reported in Eq. 5. In Eq. 5, the variation among the temperature measured over time $T(t)$ and the undisturbed ground temperature (T_{ug}) is expressed as a function of time (t) and a radial distance (r_b) from a line source with a constant heat injection rate q released along the vertical axis of the borehole. The second term in the right part represents the effects of the borehole resistance and the contribution of the surrounding ground characterized by thermal diffusivity and conductivity (α, λ). During the traditional TRT, the

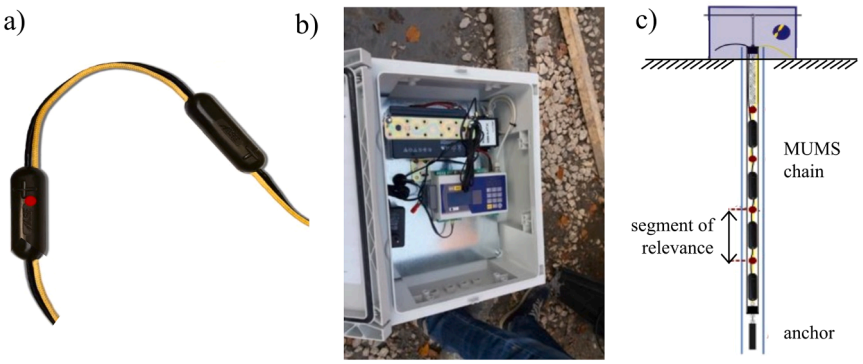

Fig. 5. a) The Thermo Link array; b) ASE801 control unit and c) scheme of the configuration (modified from https://www.aseltd.eu/it/).

measured temperature over time *T(t)* is derived as the averaged inlet and outlet temperature of the water flowing in the tubes; during the W-ETRT it is the water temperature measured by the marbles floating in the tube; during the FO-ETRT, it is the grout temperature measured by the fiber optic cable.

As many authors have shown [14,17,30], Eq. 5 can be expressed with a linear dependence of the temperature on the logarithm of time:

$$T(t) = k * \ln(t) + b \tag{6}$$

In this way, the linear correlation between the temperature variation over time and the logarithm of time is highlighted, governed by an angular coefficient denoted by the parameter *k*. The angular coefficient $k=q/4\pi\lambda$ is inversely related to the thermal conductivity, while the intercept *b* encompasses the effects of all other factors, including the borehole thermal resistance. This approximate linear trend can be assessed by graphing the temperature recorded during the heating phase against ln (t), following an initial stabilization period necessary to surpass the BHE thermal resistances, thereby achieving a steady-state condition.

The assessment of the effective equivalent thermal conductivity (λ_{eq}) of the soil, encompassing contributions from both pipe and grout, comes from reversing the angular coefficient equation:

$$\lambda_{eq} = \frac{q}{4\pi k} \tag{7}$$

The term "equivalent" is used in the estimation of thermal conductivity because, based on the initial assumption, it encompasses all heat exchange processes, including potential effects of advection in the presence of groundwater flow.

Finally, the obtained λ_{eq} allows an estimation of the thermal resistance R_b, which generally includes cumulatively all the thermal resistances within the entire borehole.

In our case, given that the tested boreholes exhibit different sections as shown in Figs. 4a and 4b, for the TRT and the W-ETRT the components contributing to thermal resistance include the following: the fluid flowing inside the pipes, the pipes walls and the filling material. Whereas, for the FO-ETRT, the thermal resistance arises solely from the copper wire and its insulation, the MUMS sensors and the borehole filling material (the Double-U tubes are absent). Therefore, we introduce a distinction among the effective borehole thermal resistance (R_b*) and the local borehole thermal resistance, (R_b) internal to the well itself, as already proposed by Lamarche et al.[22] and Javed and Spitler[20,26]. The effective thermal resistance may be expressed as time dependent (Eq. 8 derived from Eq. 5), or as a unique value (Eq. 9 derived from Eq. 6). It takes into account the whole system, including the ground in the vicinity of the BHE, thus it is affected also by the ground thermal behavior. Conversely, the local thermal resistance R_b is focused only on the borehole itself.

$$R_b^* = \frac{1}{q}(T - T_{ug}) - \frac{1}{4\pi\lambda_e}\left(\ln(t) + \ln\left(\frac{4\alpha_e}{r_b^2}\right) - \gamma\right) \tag{8}$$

$$R_b^* = \frac{1}{q}(b - T_{ug}) - \frac{1}{4\pi\lambda_e}\left(\ln\left(\frac{4\alpha_e}{r_b^2}\right) - \gamma\right) \tag{9}$$

$$R_b = \frac{T - T_{ug}}{q} \tag{10}$$

The same analytical approach (ILS) previously described has been utilized across all datasets obtained through three different methods:

1. In the case of the conventional TRT, the analysis was conducted on the temperature difference between the inlet and outlet water flowing in the BHE U-tube, yielding a single value representing the equivalent thermal conductivity of the entire stratigraphic sequence, as typically performed, and calculating the borehole thermal resistance with Eq. 9, in line with literature.
2. For the FO-ETRT, the analysis was conducted on the temporal temperature evolution measured at each depth. The measurements were taken at 0.5 m intervals, with each value representing an average across a 1 m span (0.5 m above and 0.5 m below the point). from this approach derived the averaged thermal conductivity (λ_{eq}) for the particular 1 m layer around each depth, through Eq. 7. For each reference depth, the effective borehole thermal resistance, as well has been evaluated by using Eq. 8.
3. In the W-ETRT, the analysis involved interpolating temperature values recorded by 3 (or 2 marbles) at each depth, depending on the correlation among the values provided by the different marbles, as discussed in depth in Section 4.2, with a spatial distribution of 0.1 m. This process reconstructed the temperature evolution over time for specific points and subsequently estimated the thermal conductivity (λ_{eq}) for each depth, every 0.1 m (with Eq. 7). In this case the corresponding borehole thermal resistance at each depth has been evaluated by using Eq. 10 because of the weak heating power applied during the test, as described in Section 4.3.
4. As for the direct measurements, most of them were taken using the needle probe of the ISOMET Thermal Properties Analyzer, which is suitable for silts, sands, and loose clays. Also in this case, the data analysis is based on line source theory. Only for dense or overconsolidated clays, we used the circular, plane probe, which can be connected to the same measuring device.

The analysis was conducted also on the temporal evolution of temperature measured by MUMS in the monitoring well at the depths where the sensors were installed, during the traditional TRT carried out in the nearby borehole, in order to have an independent additional dataset for comparison.

4. Results and discussion

The elaborations of the datasets acquired during the two measuring campaigns performed with the FO-ETRT and with the W-ETRT provided the following outputs, considering the traditional TRT outputs as the equivalent values for the entire stratigraphy (λ_{eq}, R_b):

1. Undisturbed temperature profile;
2. Thermal conductivity (λ_{eq}): vertical detailed profile and average value along the whole stratigraphy;
3. Borehole thermal resistance (R_b): vertical detailed profile and average value along the whole stratigraphy.

The subsequent section presents and compares the results obtained from each method.

4.1. Undisturbed temperature profile

To begin, the assessment included the evaluation of the undisturbed temperature profile and the ground temperature gradient along the depth. Fig. 6 illustrates the vertical temperature profiles measured at the onset of each campaign. The conventional TRT provides both the unique averaged temperature value, as well as the temperature profile acquired from the well log executed in the monitoring well situated 2 m away, enabling comparison with temperature profiles obtained through other methods.

All datasets concur, presenting consistent temperature profiles from a depth of 16 m onward. In the initial meters close to the surface (0–15 m), the influence of seasonal variations in air temperature is evident in the ground temperature. From 15–70 m, a zone with a low geothermal gradient exhibits a gradual and steady temperature rise with depth. Below 70 m, a consistent and nearly linear increase in ground temperature is observed, displaying a higher local gradient of about 4 °C/100 m. This trend culminates at the bottom of the borehole (125 m), where temperatures are approximately 2 degrees warmer than the upper

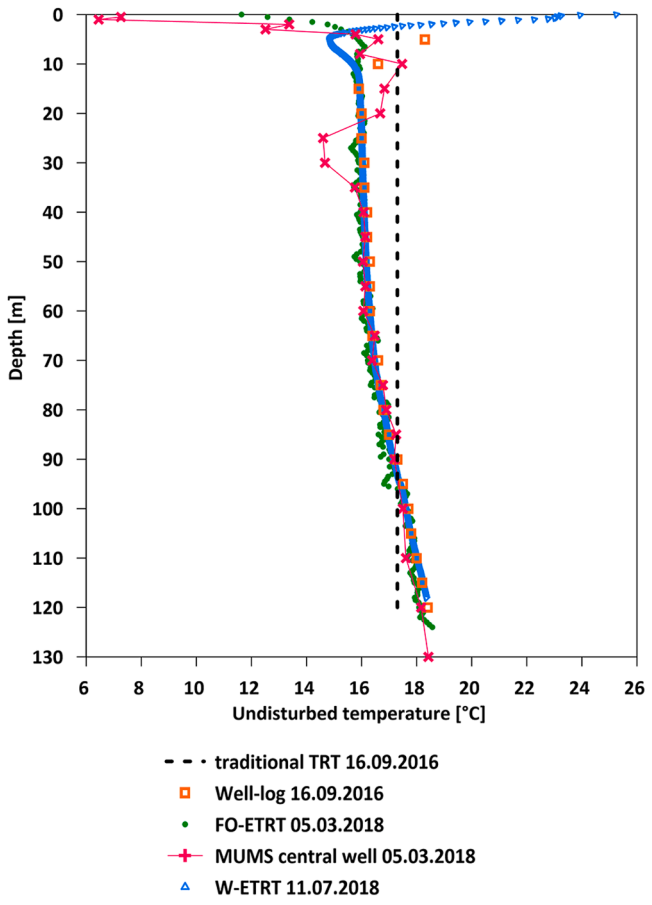

Fig. 6. Comparison of the undisturbed ground temperature profiles gained from the different testing methods.

part.

As for the MUMS, the five misaligned points between 10 and 30 m are due to some imprecisions during the calibration procedure. Table 2 presents the number of measurement points and statistical parameters for each testing method. The range of minimum and maximum temperature values notably reflects the season during which each campaign was conducted, as also indicated in Table 1.

4.2. Thermal conductivity

The thermal conductivity (λ) was determined using the calculation outlined in Eq. 7, relying on the Line Source theory detailed in Section 3.4. This involved linearly interpolating the measured temperatures against the logarithm of time. Table 3 displays the primary computed values derived from the various time series previously introduced and presents the mean thermal conductivity values (λ) derived from the W-ETRT and FO-ETRT methods, calculated over the entire depth, for comparison with the values obtained using traditional TRT. Additionally, calculating the mean values enables the determination of the standard deviation and other statistical parameters (also reported in Table 3) that describe the distribution of the measured λ values. This comparison demonstrates that, while the differences between the averaged values are relatively minor, the W-ETRT and FO-ETRT methods provide significantly more detailed information.

Fig. 7 illustrates a comparison of the vertical λ_{eq} profiles overlaid with a detailed representation of the stratigraphic sequence, categorized into six soil classes primarily based on their typical permeability and thermal properties (see also[8]). The figure presents the effective average thermal conductivity of the soil-pipe-grout system obtained from the conventional TRT, alongside the two high-resolution spatially-distributed λ_{eq} values demarcating different geological layers along the BHE vertical, as derived from FO-ETRT and W-ETRT. Furthermore, it includes the values derived from the data provided by MUMS for comparative analysis. In Table 3, the standard deviation highlights how the variable stratigraphy influences the thermal conductivity profile: it is very high for FO-ETRT and MUMS due to the strong advection detected in the lower gravel layer, which is not reached by the W-ETRT.

The coefficient of determination R^2 indicates the homogeneity of the data concerning linear interpolation: the TRT dataset exhibits the highest value, with the FO-ETRT slightly lower due to day-night oscillations in heating power, while the W-ETRT method yields a very high value, which can be attributed to the preliminary data treatment process, detailed in the following. The measurement accuracy over the extensive temperature range covered during the TRT of the MUMS sensor chain yields a low value of R^2.

For each technique, errors have been calculated by propagating the measurement accuracy of the devices used (Table 1). The errors associated with TC derived from FO-ETRT and W-ETRT are quite comparable (around 3 %), while the error from TRT is very low (<1 %) (see Table 3). The FO-ETRT error can be attributed to the oscillation in heating power, which increases the deviation from the interpolated value. In this case, the longer the test duration, the higher the error[33]. On the other hand, W-ETRT error is ascribable to the already explained difficulties in data analysis due to the very low number of data points. That heating power oscillation does not affect the TRT and, mixed with fewer variables taken into account, gives a low error on TC.

In addition, Fig. 7 also depicts the values of thermal conductivity provided by the direct measurements performed on the soil samples extracted through coring by using Isomet 2114 Thermal Properties Analyzer. The results of the direct measurements correlate very closely with the in-situ measurements apart from a few outliers. The direct measurements take into account only the thermal conductivity, and there is no influence of advection provided by the groundwater flow; in addition, they refer to a defined depth sample, and are not averaged values. Moreover, some differences can be ascribed to water loss during the soil sample collection, the unconfinement during the sampling operations leading to structure and density changes, and scale effects (see also[11]).

The traditional TRT dataset was analyzed starting 12.50 hours after the heating phase commenced, meeting the time criterion, where $F_0 \geq 5$ [17]. Following an initial floating trend, the thermal conductivity of the soil-pipe-grout system stabilized at 1.68 W/(m·K), chosen as the average

Table 2
Number of measurements points and temperature statistical parameters for each testing method.

	Measuring points #	Test date	T max (°C)	T mean from ground level (°C)	T mean from the depth of 16 m (°C)	T min (°C)
TRT	1	16.09.2016		17.3	17.3	
FO-ETRT	251	05.03.2018	18.6	16.5	16.7	8.5
W-ETRT	1182	11.07.2018	25.2	16.7	16.7	14.8
MUMS	28	05.03.2018	18.4	15.6	16.6	6.4
Well-log	24	16.09.2016	18.4	16.9	16.9	15.9

Table 3
Number of measurement points and thermal conductivity statistical parameters for each testing method.

	Measuring points #	λ max (W/m·K)	λ mean (W/m·K)	λ min (W/m·K)	St. Dev.	R^2	Mean Error, %	Min Error	Max Error
TRT	1	1.68	1.68	1.68	-	0.998	0.0147 (0.88 %)	-	-
FO-ETRT	248	8.81	2.01	1.27	0.66	0.938	0.0598 (3.32 %)	0.0045	0.1329
W-ETRT	1067	2.78	1.62	1.04	0.23	0.996	0.0451 (2.94 %)	0.0145	0.1022
MUMS	28	5.42	1.74	1.02	0.75	0.882	-	-	-

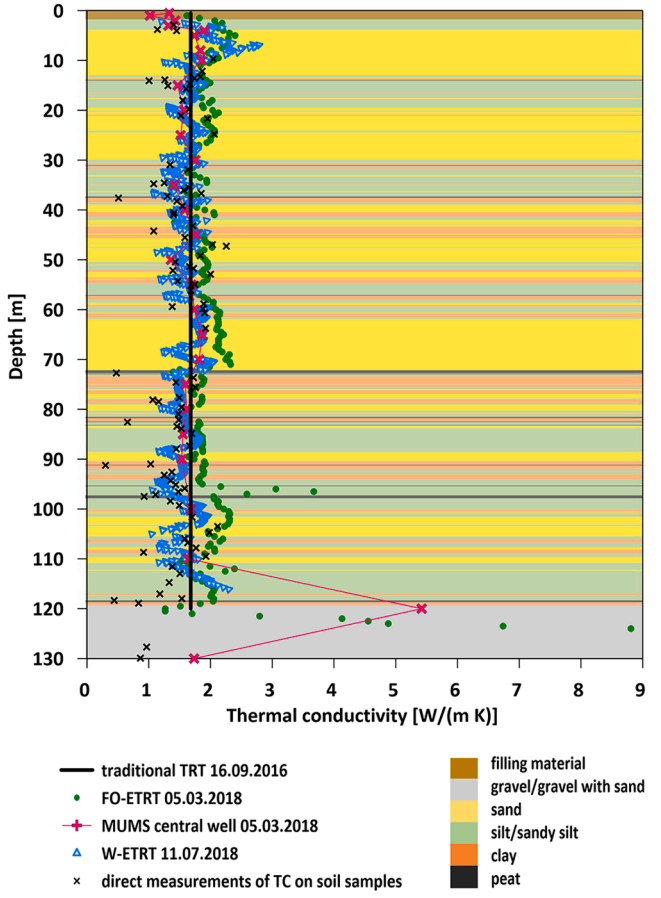

Fig. 7. Comparison of the ground thermal conductivity profiles gained from the different testing methods and correlation with the geological layers.

value for λ_{eq}.[17]

In the case of the FO-ETRT, after filtering with a low pass filter, we applied the common calculation method as $F_0 = 5$, that is in our case after 10 hours of heating. Given the day-night heating power oscillation, we adjust the time range to cover almost three complete fluctuations until the end of the heating, in order to reduce the error.

Conversely, for W-ETRT the process was more complex due to the low number of measuring points for each depth, during heating. Temperature measurements are at 17.2, 23, 33, 72.65 hours from the beginning of the heating phase. However, the value at 17.2 hours belongs to the transient initial heating phase and it was therefore excluded from the calculations. Therefore, only three points can be considered acceptable under the ILS theory assumptions and consequently used to evaluate the thermal conductivity at each depth. The coherence between the three measured values was assessed using the R^2 function on a linear interpolation. The results suggest relying on the last two points for calculating thermal conductivity and including the value measured at 23 hours only if it does not deviate more than 1 % from the linear regression line. This indicates that at the 23-hour mark a steady-state condition had not been fully reached at the tested depths (e.g., at depths of 2.10 m, 58.5 m, and from 116 m to 118 m).

Fig. 8 presents a direct comparison between the temperature recorded over time by both methods at a specific depth (41 m depth) superimposed to the temperature measures at the BHE inlet and outlet during the traditional TRT, for comparison. First, the two graphs clearly illustrate the substantial difference in the amount of data obtained by each technique: during heating, FO-ETRT records over 5600 measurements, similarly to the traditional TRT, whereas W-ETRT captures only three valid values. Consequently, FO-ETRT enables a comprehensive identification of the heating curve, facilitating the calculation of an interpolation curve for thermal conductivity assessment, while W-ETRT provides a suggestive yet limited curve due to the scarcity of data points. In the figure, the red dashed lines interpolate the measured values in the last linear part of the heating curve, when the steady-state conditions are achieved.

Moreover, the graphs highlight the discrepancy in the heating power applied by the two methods to stimulate the ground, resulting in different temperature increases. The intensity of the heating power affects the clarity of the signal: the W-ETRT heating power is extremely weak compared to the other two, and this is extremely relevant especially for the calculation of the R_b. This is highlighted also in Fig. 8b where the temperature values measured at 41 m depth by W-ETRT and

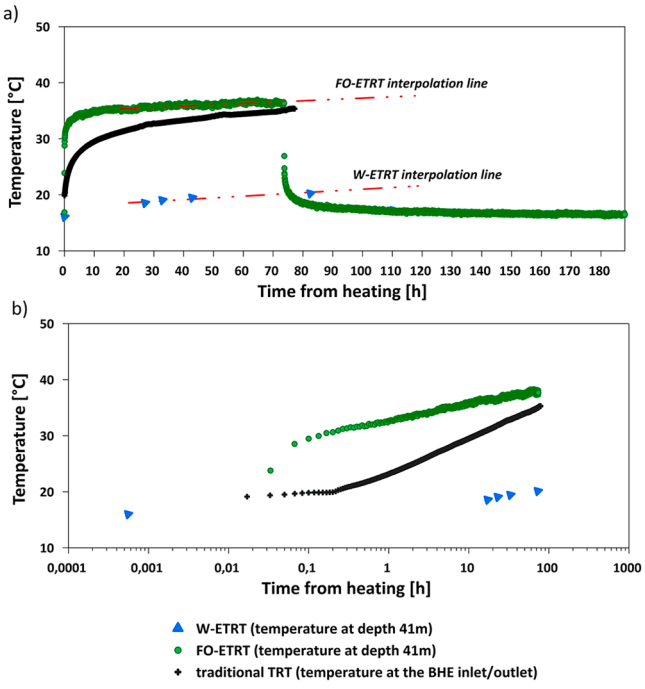

Fig. 8. : Temperature measurements over time at 41 m (a) by using W-ETRT and FO-ETRT and their respective interpolation lines (in the last linear part of the heating curve, when the steady-state conditions are achieved). The temperature measured at the BHE inlet and outlet is also reported for comparison; in (b) temperature values measured at depth 41 m by W-ETRT and FO-ETRT plotted against ln(t), together with the temperature measured at the BHE inlet and outlet during the traditional TRT.

FO-ETRT are plotted against ln(t), together with the temperature measured at the BHE inlet and outlet during the traditional TRT.

The slope of the linear interpolation is the highest for the TRT, proportional to the higher injected heat rate (Table 1); for the other two, the slope is comparable as well as the injected heat rate despite the different temperature range covered during the test. The maximum reached temperature is equal to 37.8 °C for the FO-ETRT, 35.3 °C for the traditional TRT and 20.1 °C for W-ETRT.

The mean values of thermal conductivity across the entire vertical profile are relatively close to those provided by the traditional TRT. However, the new techniques capture significant variations corresponding to different soil types. The FO-ETRT and W-ETRT vertical profiles of λ exhibit considerable detail. Despite minor discrepancies due to differences in soil thickness at which the datasets are referenced (0.1 m for W-ETRT), both techniques successfully identify subsoil layers characterized by high thermal exchange capacity. For instance, sandy and gravelly layers at depths of 2–15 m, 22–28 m, 62–72 m, 102–108 m, and the deep aquifer with significant groundwater flow between 121 m and 129 m are well captured by the FO, which reaches this depth. W-ETRT reached a shallower depth and in the lower part is very close to the final part of the U-tube, thus increasing the uncertainties in the measured values.

Lower values of thermal conductivity identified by the W-ETRT may correspond to thicker layers of massive clay or peat, such as at 72 m and 98 m. The highest values are recorded in the deep gravelly aquifer driven by groundwater flow, with FO-ETRT showing λ=8.81 W/(m·K), and the MUMS dataset registering λ=5.42 W/(m· K) for this layer. Additionally, differences arise due to the assumption of heat exchange solely in the radial direction, as postulated by the ILS theory. Particularly near an aquifer, ground conditions allow for advective heat exchange in both radial and vertical directions within the surrounding layers.

Differences in mean values could also arise from varying lengths probed by each technique: the traditional TRT stopped at 120 m, W-ETRT investigated down to 118 m (to protect marbles), FO-ETRT ended at 124 m, and the last sensor of the MUMS chain is installed at 130 m.

The deeper layers from 120 m to 130 m have a noticeable impact. The results obtained with the FO-ETRT and the MUMS chain, that intersect the deeper aquifer, highlight that in this site longer boreholes, reaching 130 m and not only 120 m, would significantly improve borefield heat exchange capacity and the overall system efficiency.

This result highlights the importance of conducting high-resolution ETRT during the design phase to optimize individual BHE lengths.

4.3. Borehole thermal resistance

Fig. 9 directly compares the vertical profile of R_b, derived by the measurements obtained with the three different tests. The borehole thermal resistance is evaluated as described in Par. 3.5, by taking into account the different cross sections proper of each tested borehole (shown in Figs. 4a and 4b). Obviously, the traditional TRT dataset provides a unique value of R_b equal to 0.101 (m·K)/W, which is used as reference. The vertical profile obtained from the W-ETRT dataset fluctuates around the TRT value, indicating some variability. In contrast, the FO-ETRT profile displays consistently higher values (approximately 0.2–0.3 (m·K)/W) across the entire depth. This can be ascribable to the different cross sections of the tested wells: traditional TRT and the W-ETRT were performed in boreholes with the same cross section (represented in Fig. 4b) whilst the FO-ETRT was performed in the monitoring well (whose section is represented in Fig. 4a). Nevertheless, all of them are reasonable for the corresponding tested well set-up. Table 4 summarizes the statistical values of R_b, as well as the minimum, maximum, and mean errors.

As pointed out in Fig. 9, the monitoring well effectively offers higher thermal resistances. This is due to a combination of the following three effects: the geometry and materials constituting the cross section, the

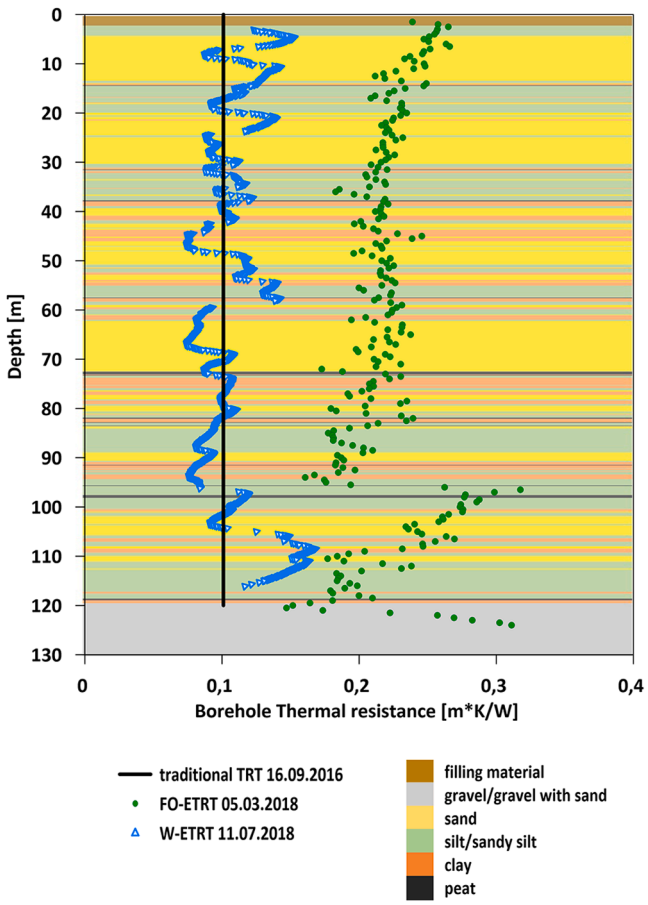

Fig. 9. Comparison of the borehole thermal resistance R_b profiles and related statistics.

extension of the heater side surface, and the heater material itself. Please note that the monitoring well had an initial drilling diameter of 152 mm, exactly like the Double-U BHEs. During the drilling operations, a 103 mm wide plastic cylinder for piezometric tests was inserted into the hole to sustain the excavation during the installation procedures of the monitoring apparatus.

In the FO-ETRT technique, the heater is the copper wire within the fibre optic cable, and the cross section includes, in addition to the hybrid fiber optic cable, also the cables' coating, the MUMS system, the plastic tube and a wider thickness of filling grout, because of the absence of the Double-U tubes. Even if this configuration offers higher thermal resistance, the FO-ETRT induces a significant temperature increase in the surrounding ground, with respect to the one produced by W-ETRT (22.8 °C and 5.63 °C, respectively, as reported in Table 1). A significant increase in the ground temperature is necessary to enable the evaluation of R_b (by using Eqs. 8 and 9).

The R_b vertical profile achieved from the FO-ETRT shows an undulating behaviour with the stratigraphic sequence and all the significant variations can be associated to stratigraphy variations resulting in different grout expansion and structure. The graph shows a general decreasing trend in the first sandy layers down to the depth of 38 m, followed by a sort of stabilization down to 82 m, corresponding to a continuous alternation of sandy and silty deposits, finer than the shallower ones. A new decreasing trend is observable down to a depth of 95 m, corresponding to a series of finer layers (silt and clays). At 95 m an abrupt significant peak is measured in correspondence to a layer of peat and silt; it can be ascribable to the higher horizontal infiltration of grout into the subsoil due to the loose materials or planar structure and high porosity resulting in increasing grout diameter. Afterwards, the R_b

Table 4
Number of measurement points and borehole resistance statistical parameters for each testing method.

	Measuring points #	R_b max (m·K/W)	R_b mean (m·K/W)	R_b min (m·K/W)	St. Dev.	Mean Error, %	Min error	Max Error
TRT	1	-	0.101	-		0.010 (0.94 %)	-	-
FO-ETRT	248	0.318	0.220	0.147	0.028	0.0035 (1.64 %)	0.0034	0.0041
W-ETRT	1067	0.168	0.108	0.074	0.023	0.057 (5.5 %)	0.0056	0.0063

profile decreases with analogous oscillations reaching values that are similar to the ones before the peak and, finally, the profile drastically increases in correspondence to the deep aquifer with high groundwater flow where the extremely high advection exceeds the theoretical assumptions of the interpretative ILS model.

Conversely, during the W-ETRT, the heating power is provided by a copper cable warming up the water inside one of the 4 legs of the Double-U tube, while the measuring marbles are sinking in one of the other legs. The cross section offering thermal resistance is constituted by the water in the tube itself, the pipes and grout.

Moreover, the provided power during W-ETRT is 18 W/m, significantly lower than that injected during the other tests, equal to 23 and 58 W/m during FO-ETRT and traditional TRT, respectively. It is sufficiently high to overcome all the section thermal resistances and thus estimate the ground thermal conductivity, but it is too weak for the evaluation of the thermal borehole resistance with the standard methods (Eq. 8 and Eq. 9). In the W-ERT, the rate between power and time is so low that, for some soil layers, the second negative term in Eqs. 8 or 9 is higher than the first one, resulting in a negative value for R_b*, that is not-physical. For this reason, we introduce Eq. 10 to obtain a valid local R_b value, as previously proposed by Lamarche et al.[22] and Javed and Spitler[20], where the second term is missing. This formula does not take into account the surrounding ground effects so that the resulting local R_b value is strictly related only to the borehole itself.

The variations of the thermal resistance profile do not display a trend associated to the stratigraphy but they seem more ascribable to a non-homogeneous grout distribution.

Table 4 shows that, for traditional TRT and FO-ETRT, the mean errors are around 1 %, lower than W-ETRT error that is equal to 5.5 %.

To sum up, from this comparison, the FO-ETRT technique appears to be more reliable in evaluating the R_b vertical profile (if applied in a Double-U BHE), despite being applied to a monitoring well in this study case, and not to a standard BHE.

4.4. Critical methods comparison

The two methods under comparison, i.e. the hybrid fiber optic cable (FO-ETRT) and the Geosniff marbles (W-ETRT), provide temporal temperature assessments along a vertical profile, allowing for the analysis of variations in thermal conductivity. Yet, they rely on different measurement methodologies, each presenting its own distinct benefits and limitations, as detailed below.

- Regarding data spatial frequency, the FO cable captures data at a high spatial frequency along its length but delivers values at 0.5 m intervals, each calculated as an average within a 1 m window. In contrast, the marbles (W-ETRT) provide temperature values at 0.1 m intervals specific to each depth (without averaging). Therefore, the Geosniff technique might capture subtle thermal behaviours, particularly in layers of minimal thickness.
- As for the precision of the measurement depth, the fiber optic cable creates a continuous line of measurement sensors positioned at fixed intervals throughout its length, sealed within the borehole ‘s grout; thus, the measurement depth is fixed and well-known. In contrast, the W-ETRT marbles measure local water temperature while floating in the U-tubes’ water and estimate the depth of each temperature value through water pressure measurements. These readings could be affected by varying water temperatures influencing water density, which fluctuates differently over time at different depths. Moreover, also water movements caused by the floating marble might lead to imprecise depth identification. These potential sources of imprecision become more pronounced with increasing depth of the layers under investigation. Nevertheless, both methods provide an accurate temperature profile over the entire investigated depth despite the different spatial accuracy.
- Regarding temporal resolution, FO-ETRT provides data with an extremely high temporal resolution, offering a detailed temperature variation curve over time. Conversely, the Geosniff technique (W-ETRT) utilizes a limited number of marbles (i.e. time sampling) that are released at previously set intervals. In our case, we had only 6 marbles in total. Throughout the heating phase, the availability of only three temperature values per depth posed a significant limitation for computing thermal conductivity by applying the line source approach. This limitation was further pronounced across nearly 100 depth points, where the interpolation of data was not reliable, so that only the last two datasets were used, as already explained in Section 4.2. To mitigate this issue, employing an additional one or two marbles to measure temperature during the heating phase is suggested to enhance accuracy. Furthermore, FO-ETRT provides values also during the recovery phase, leading to potential additional studies and investigation.
- Concerning the heating methods employed, in general both measurement techniques can utilize a heating copper cable electrically charged (as seen with the hybrid FO cable in this scenario or inserted in the other leg of the Double U-tube) or a water tank injecting hot water into the BHE, similar to the traditional TRT. The former method offers a more uniform and consistent heating source along the cable due to the copper’s steady thermal resistance and heating supply. Conversely, the latter method provides an uneven heating source, stronger in the shallower ground layers and progressively becoming weaker. However, electrically powering the copper wire requires a stable power supply and might experience instability if concurrent uses operating in the building site affect it. In this specific case, both tests utilized an electrically charged copper cable for heating purposes. FO-ETRT employed a hybrid FO, reaching a maximum temperature of 40 °C, positioned close to the measuring cable, in line with the assumptions made by the ILS. Meanwhile, during W-ETRT, the heating cable was placed within the other leg of the Double U-tube and reached a maximum temperature of 25°C, thus resulting in a weaker ground thermal solicitation.
- The geological setup of the test site presents a significant challenge due to the existence of extremely thin layers with alternating layers of aquifers and aquitards. The W-ETRT method may encounter difficulty in identifying advection in aquifers of low thickness and with low groundwater flow, where the advective signal is minimal and it is only slightly captured by the floating marble due to the short time spent by the sensor in that layer (with a descent of 6.5 m/min). Unlike FO-ETRT, which is continuously sensitive, meaning it can take continuous measurements along its entire length throughout the entire measurement period, capturing the full variety throughout the entire depth and the entire 72-hour duration. Thus, the W-ETRT technique might prove more effective in geological settings marked by thicker layers. Alternatively, it could be better suited for

geological environments with thinner layers but minimal variations in groundwater fluxes.
- On the other hand, in the case of very thin layers (<1 m) with significant groundwater flow or peat layers of very limited thickness where an abrupt variation in thermal conductivity (TC) is expected, the FO-ETRT may be less reliable. This is because it provides smoothed values obtained by averaging data measured within a 1 m window. Although W-ETRT is sensitive to certain unknown fluctuations, it seems more adept at detecting thin strata due to its higher spatial resolution.
- The presence of massive clay or organic materials such as peat, in conjunction with irregular and heterogeneous layers within the stratigraphic sequence, correctly leads to a considerable reduction in TC detected by both techniques. In our case, these layers are of limited thickness and W-ETRT demonstrates a better capability to capture these variations. FO-ETRT captures clay/peat layers as well, although its sensitivity might vary based on layer thickness, due to its averaging of temperature above 1 m wide.
- As for the vertical profile R_b evaluation, the variations of the thermal resistance profile display a trend only slighted associated to the stratigraphy and probably ascribable to a non-homogeneous grout distribution. Correctly, the result is strongly affected by the section of the investigated well. The theory supporting the estimation of R_b applied to FO-ETRT or W-ETRT measurements needs further investigation, because the formulas used for the traditional TRT are based on several theoretical assumptions that may be not valid in ETRT configurations characterized by different heating methods and different well cross sections. For this reason, we proposed different calculation methods.
- Finally, from logistical and economic viewpoints, the FO-ETRT involves more complexity, requiring a dedicated FO cable and a proper interrogator, which can be quite expensive. Conversely, Geosniff equipment is lighter, offer easiers integration into existing boreholes and it is usually cheaper. The time commitment for both techniques is similar, as both require a minimum of 72 hours of thermal solicitation, following the TRT ASHRAE and VDI guidelines.[5,34,36]

5. Conclusions

To achieve high-performance BHEs, the design phase often demands a comprehensive understanding of the local thermal properties of the ground, intricately linked to site-specific lithological and hydrogeological conditions. Therefore, this study aimed at evaluating and comparing the response and attributes of both novel and standard TRT measurements conducted in the field.

To obtain depth-distributed effective thermal parameters of the ground, it is essential to monitor its thermal evolution during an appropriate thermal excitation. Technologies such as FO-ETRT (here performed with Optical Fiber GeoDTS and APSensing® interrogator) and wireless data transmission W-ETRT (here performed through GEOsniff®) enable a high-resolution, spatially-distributed representation of the subsoil's thermal properties along the BHE.

The previously discussed data highlights the advantages and disadvantages of each technique:

- In contrast to the conventional TRT, both FO-ETRT and W-ETRT are capable to deliver detailed, spatially-resolved thermal property estimation, so that they are particularly valuable in environments marked by complex stratigraphic sequences and, consequently, varying thermal responses layer by layer. In particular in presence of an aquifer with significant groundwater flow, the heat transfer is dominated by convection rather than conduction heat transfer process. The FO-ETRT, which reached the depth of the deep aquifer with high groundwater flow, evidences this phenomenon, showcasing a peak value of apparently high TC from a depth of 120 m.
- FO-ETRT outcomes exhibit a 0.5 m resolution at fixed depths, presenting values averaged within a 1 m window. It appears more sensitive to the presence of groundwater flow, which may be due to the higher thermal power solicitation. The method involves higher power resulting in a clearer signal. However, in this configuration it necessitates installing the hybrid cable within the borehole during construction, during sealing operations with grout throughout its depth. This process can be costly, mainly due to the cable expenses (cable to lose) and the need for an interrogator (also the other techniques used a proper interrogator, but usually cheaper).
- The tested W-ETRT instrument measured temperatures at 0.1 m intervals, thus providing a higher spatial resolution, although these values might be impacted by possible inaccuracies in water pressure evaluation. The accuracy of temperature measurement remains consistent regardless of spatial resolution and sampling time but, at some depths, it is necessary to check the consistency of the data acquired at different times due to uncertainty connected to the calculation of the depth.
- As for the detection of different geological strata, both techniques here analysed clearly identify the sandy layers characterized by high thickness, homogeneity and higher thermal conductivity, as well; they both are also capable of detecting the alternation of thin silt, silty-sand, clayey-silt layers and the negative peak of peat or, in general, the presence of organic matter.
- As for the layers of limited thickness (<1 m), the W-ETRT appears more effective due to its higher spatial resolution. FO-ETRT may be less reliable because, despite it is continuously sensitive along its entire length, it provides smoothed values obtained by averaging data measured within a 1 m window.
- In cases of layers with significant groundwater flow, the FO-ETRT seems more reliable due to the large amount of data registered over time and to the stability of the optic fiber. Conversely, the advective effect captured by the sinking marble is minimal due to the short time spent by the marble to cross each layer, especially if the layer thickness is limited.
- A notable distinction among FO-ETRT and W-ETRT lies in the volume of acquired data: the thousands of temperature values obtained through FO-ETRT offer extensive data analysis potential, not only during the heating phase but also in the thermal relaxation period. Moreover, installing the hybrid FO cable in a monitoring well, as demonstrated in this study, enables subsequent field campaigns to monitor underground thermal behaviour over time, even linked to the geothermal plant operation conditions.

In conclusion, both the innovative techniques seem capable of identifying significant variations in the vertical profile of the thermal conductivity caused by different soil layers' thermal behaviour or groundwater conditions, making both of them suitable, each with its own strengths and weaknesses, for providing the depth-resolved subsoil thermal characterization to optimize the design of a new BHEs field. Future developments may consider the application of new analytical solutions that incorporate the advection term to analyze the measured datasets, thus allowing for the distinction of groundwater flow contributions to heat exchange. This approach could be particularly important in the gravelly layer encountered at the bottom of the BHE. In addition, an interesting development may be the application of the theory of temperature-dependent resistances as suggested by Albers et al.[3], to adjust the variation of the specific heat loads along the length of the heating cable, which are expected to be more significant for hydrogeological conditions with varying groundwater flow (i.e., at a study site with alternating layers of aquifers and aquitards), as in the case here presented.

Declaration of Competing Interest

The authors declare that they have no known competing financial interests or personal relationships that could have appeared to influence the work reported in this paper.

Data availability

Data will be made available on request.

References

[1]. Acuña J, Mogensen P, Palm B. Distributed thermal response tests on a multi-pipe coaxial borehole heat exchanger. *HVAC R Res*. 2011;17:1012–1029. https://doi.org/10.1080/10789669.2011.625304.

[2]. Acuña J, Palm B. Distributed thermal response tests on pipe-in-pipe borehole heat exchangers. *Appl Energy*. 2013;109:312–320. https://doi.org/10.1016/j.apenergy.2013.01.024.

[3]. Albers A, Steger H, Zorn R, Blum P. Evaluating an enhanced thermal response test (ETRT) with high groundwater flow. *Geotherm Energy 2024*. 2024;12(1):1.

[4]. Antelmi M, Alberti L, Angelotti A, Curnis S, Zille A, Colombo L. Thermal and hydrogeological aquifers characterization by coupling depth-resolved thermal response test with moving line source analysis. *Energy Convers Manag*. 2020;225, 113400. https://doi.org/10.1016/j.enconman.2020.113400.

[5]. ASHRAE Handbook—HVAC Applications. Atlanta, Georgia: American Society of Heating, Refrigerating and Air-Conditioning Engineers; 2011:1242.

[6]. Austin WA, Yavuzturk C, Spitler JD. Development of an in situ system for measuring ground thermal properties. *ASHRAE Trans*. 2000;106:356–379.

[7]. Banks D. *An Introduction to Thermogeology: Ground Source Heating and Cooling*. Oxford, UK: Blackwell Publishing, Ltd; 2008. https://doi.org/10.1002/9781444302677.

[8]. Dalla Santa G, Galgaro A, Sassi R, et al. An updated ground thermal properties database for GSHP applications. *Geothermics*. 2020;85, 101758. https://doi.org/10.1016/j.geothermics.2019.101758.

[9]. Dalla Santa G, Galgaro A, Tateo F, Cola S. Modified compressibility of cohesive sediments induced by thermal anomalies due to a borehole heat exchanger. *Eng Geol*. 2016;202:143–152. https://doi.org/10.1016/j.enggeo.2016.01.011.

[10]. Dalla Santa G, Galgaro G, Tateo A, Cola F. S. Induced thermal compaction in cohesive sediments around a borehole heat exchanger: laboratory tests on the effect of pore water salinity. *Environ Earth Sci*. 2016;75:1–11. https://doi.org/10.1007/s12665-015-4952-z.

[11]. Dalla Santa G, Pasquier P, Schenato L, Galgaro A. Repeated ETRTs in a complex stratified geological setting: High-resolution thermal conductivity identification by multiple linear regression. *J Geotech Geoenviron Eng*. 2022;148(4), 04022007. https://doi.org/10.1061/(ASCE)GT.1943-5606.0002724.

[12]. Dalla Santa G, Peron G, Galgaro F, et al. A. Laboratory Measurements of Gravel Thermal Conductivity: An Update Methodological Approach. *Energy Procedia*. 2017:671–677. https://doi.org/10.1016/j.egypro.2017.08.287.

[13]. de Sousa Figueira J, Nachbaur S, Wehinger S, Bourne-Webb P. The Implementation and Comparison of Conventional and Enhanced Borehole Thermal Response Tests: A Case Study. *Energies*. 2024;17(13):3161.

[14]. Eklöf C., Gehlin S. A Mobile Equipment for Thermal Response Test Testing and Evaluation. Doctorial Thesis. 1996.

[15]. Fujii H, Okubo H, Itoi R. Thermal response tests using optical fiber thermometers. *: GRC 2006 Annu Meet: Geotherm Resour-Secur Our Energy Future*. 2006:545–551.

[16]. Galgaro A, Dalla Santa G, Zarrella A. First Italian TRT database and significance of the geological setting evaluation in borehole heat exchanger sizing. *Geothermics*. 2021;94, 102098. https://doi.org/10.1016/j.geothermics.2021.102098.

[17]. Gehlin S., Nordell B. Determining undisturbed ground temperature for thermal response test. ASHRAE Trans. ISSN 0001-2505 151–156. 2003.

[18]. Ingersoll L, Adler F, Plass H, Ingersoll A. Theory of earth heat exchangers for the heat pump. *ASHVE Trans*. 1950;56:167–188.

[19]. Ingersoll LR, Zobel OJ, Ingersoll AC. Heat conduction with engineering, geological, and other applications. *Phys Today, Thames Hudson Ed, Lond*. 1955;8:17. https://doi.org/10.1063/1.3061951.

[20]. Javed S, Spitler JD. *Calculation of borehole thermal resistance. in Advances in ground-source heat pump systems*. Woodhead Publishing; 2016:63–95. https://doi.org/10.1016/B978-0-08-100311-4.00003-0.

[21]. Kelvin, W.T.. Mathematical and physical papers. London: Cambridge University Press. 1882.

[22]. Lamarche L, Kajl S, Beauchamp B. A review of methods to evaluate borehole thermal resistances in geothermal heat pump systems. *Geothermics*. 2010;39(2):187–200. https://doi.org/10.1016/j.geothermics.2010.03.003.

[23]. Lehr C, Sass I. Thermo-optical parameter acquisition and characterization of geologic properties: a 400-m deep BHE in a karstic alpine marble aquifer. *Environ Earth Sci*. 2014;72:1403–1419. https://doi.org/10.1007/s12665-014-3310-x.

[24]. Luo J, Rohn J, Xiang W, Bertermann D, Blum P. A review of ground investigations for ground source heat pump (GSHP) systems. *Energy Build*. 2016;117:160–175.

[25]. Marcolla A, Miola A, Mozzi P, et al. Middle Pleistocene to Holocene palaeoenvironmental evolution of the south-eastern Alpine foreland basin from multi-proxy analysis. *Quat Sci Rev*. 2021;259, 106908. https://doi.org/10.1016/j.quascirev.2021.106908.

[26]. Marcotte D, Pasquier P. On the estimation of thermal resistance in borehole thermal conductivity test. *Renew Energy*. 2008;33(11):2407–2415. https://doi.org/10.1016/j.renene.2008.01.021.

[27]. Mascarin L, Garbin E, Di Sipio E, et al. A.Selection of backfill grout for shallow geothermal systems: materials investigation and thermo-physical analysis. *Constr Build Mater*. 2022;318, 125832. https://doi.org/10.1016/j.conbuildmat.2021.125832.

[28]. Mogensen P. Fluid to duct wall heat transfer in duct system heat storages. *Doc - Swed Counc Build Res*. 1983.

[29]. Perego R, Dalla Santa G, Galgaro A, Pera S. Intensive thermal exploitation from closed and open shallow geothermal systems at urban scale: unmanaged conflicts and potential synergies. *Geothermics*. 2022;103, 102417. https://doi.org/10.1016/j.geothermics.2022.102417.

[30]. Sanner B, Hellström G, Spitler J, Gehlin S. *Thermal Response Test, current status and world-wide application*. Melbourne, Australia: In: Proceedings World Geothermal Congress; 2005.

[31]. Schenato L. A review of distributed fibre optic sensors for geo-hydrological applications. *Appl Sci*. 2017;7(9):896. https://doi.org/10.3390/app7090896.

[32]. Schwarz H, Badenes B, Wagner J, Cuevas JM, Urchueguía J, Bertermann D. A case study of thermal evolution in the vicinity of geothermal probes following a distributed TRT method. *Energies*. 2021;14:2632. https://doi.org/10.3390/en14092632.

[33]. Song W, Wang J, Jin Y, Zheng C, Zhang B. Optimization of the thermal response test under voltage fluctuations based on the infinite line source model. *Renew Energy*. 2023:203731–203740. https://doi.org/10.1016/j.renene.2022.12.094.

[34]. VDI, 2010. VDI-standard. VDI 4640 Blatt 1. Thermal Use of the Underground.

[35]. Vélez Márquez MI, Raymond J, Blessent D, et al. Distributed thermal response tests using a heating cable and fiber optic temperature sensing. *Energies*. 2018;11(11):3059. https://doi.org/10.3390/en11113059.

[36]. Verein Deutscher Ingenieure. *VDI 4640 Blatt 5 Thermal use of the subsurface - Thermal Response Tests*. 2010.

[37]. Vieira A, Alberdi-Pagola M, Christodoulides P, et al. Characterisation of ground thermal and thermo-mechanical behaviour for shallow geothermal energy applications. *Energies*. 2017;10(12):2044. https://doi.org/10.3390/en10122044.

[38]. Wilke S, Menberg K, Steger H, Blum P. Advanced thermal response tests: A review. *Renew Sustain Energy Rev*. 2020;119, 109575. https://doi.org/10.1016/j.rser.2019.109575.

[39]. Zhang B, Gu K, Shi B, et al. Actively heated fiber optics based thermal response test: a field demonstration. *Renew Sustain Energy Rev*. 2020;134, 110336. https://doi.org/10.1016/j.rser.2020.110336.

[40]. Zhang B, Gu K, Wei Z, et al. Governing factors for actively heated fiber optics based thermal response tests. *Renew Energy*. 2023;219, 119461.